Carbohydrate Research 559 (2026) 109743

Contents lists available at ScienceDirect

Carbohydrate Research

journal homepage: www.elsevier.com/locate/carres

Lipooligosaccharide architecture in *Acinetobacter modestus* CM11G: a non-pathogenic strain

Immacolata Speciale [c], Luisa Sturiale [b], Angelo Palmigiano [b], Anna Notaro [a,*]

[a] Department of Chemical Sciences, University of Napoli Federico II, I-80126, Napoli, Italy
[b] CNR, Institute for Polymers, Composites and Biomaterials, 95126, Catania, Italy
[c] Department of Chemical Sciences, University of Naples Federico II, Via, Cintia, 80126, Naples, Italy

ARTICLE INFO

Keywords:
Gram-negative bacterium
Lipooligosaccharide
OS region
Lipid A
Structural determination
NMR
MALDI

ABSTRACT

The *Acinetobacter* genus comprises a multitude of species that have been isolated from both environmental and clinical samples. In recent years, the scientific community has expended considerable effort in characterising the structures of the capsular polysaccharides and lipooligoaccharides (LOS) of *A. baumannii*, given the increasing mortality rate caused by this species. Comparatively little research has been undertaken for the non-pathogenic species.

In the present study, we describe the first case of isolation and identification of the LOS molecule of *Acinetobacter modestus* CM11G, a Gram-negative bacterium colonising the intestinal crypts of a healthy mouse. By combining spectroscopic and spectrometric analyses with chemical derivatisations, we were able to determine the structure of the entire LOS. The lipid A moiety is composed mainly of hepta-acylated species, a characteristic also observed in other *Acinetobacter* species. It is extended with a disaccharide of Kdo, which acts as a bridge between the lipid A and the oligosaccharide portion. Indeed, the internal Kdo residue is linked at position *O*-5 with a novel tetrasaccharide composed of βGlcN(1→2)-βGal(1→6)-αGlc(1→, where the glucose is further substituted at position *O*-4 with a terminal β-Glc. In contrast, the external Kdo residue does not undergo further substitution, contrary to what generally occurs in the LOS of *A. baumannii*.

1. Introduction

In recent years, over 144 species of the genus *Acinetobacter* have been identified [1], exhibiting both ecological and clinical significance. These bacteria are classified as Gram-negative, characterised by an oval shape, lack of motility, and a non-fermentative metabolic profile [1]. For a considerable period, these organisms have been considered as environmental bacteria, isolated from soil and water, and playing an important role in degrading pollutants such as diesel [2] and phenol [3]. However, the number of *Acinetobacter* species identified as the cause of nosocomial infections is increasing. Indeed, *A. baumannii* has been identified as the primary causative agent of various diseases, including pneumonia, meningitis, sepsis, and others, with a high mortality rate [4]. In addition, the presence of two species of *Acinetobacter* (namely *A. radioresistant* CM38.2 and *A. modestus* CM11G) has been identified in a Crypt-Specific Core Microbiota (CSCM) in the caecum and proximal colon of laboratory-reared healthy mice [5,6]. Interestingly, these species, together with other bacteria colonising the CSCM, such as *Delftia acidovorans* and *Stenotrophomonas maltophilia*, have been considered crypt guardians since they preserve the epithelial crypt regeneration apparatus [6]. Additionally, Naito et al. [7] demonstrated that lipopolysaccharide molecules (LPSs) produced by these Gram-negative bacteria played a central role in the epithelial regeneration process. All these findings, together with the fact that scientific evidence shows that LPS can act as toxic or benign molecules depending on their chemical composition [8], explain why structural determination is a crucial step in identifying the structure-function correlation. In the frame, we have contributed to the characterisation of the LPS structure of the LPS from *Delftia acidovorans,* another Gram-negative bacterium colonising the CSCM [9]. In this study, the structure of the lipooligosaccharide (LOS) of *A. modestus* CM11G has been elucidated.

Contrary to LPS, the LOS biomolecule is composed of two regions [7]: a conserved phosphoglycolipid (lipid A) and a rather short oligosaccharide chain (core OS region), lacking the surface-exposed O-polysaccharide (O-antigen). The canonical OS region is organized into i) an inner core, which is highly conserved and composed of Kdo

* Corresponding author.
E-mail address: anna.notaro@unina.it (A. Notaro).

https://doi.org/10.1016/j.carres.2025.109743
Received 18 September 2025; Received in revised form 6 November 2025; Accepted 6 November 2025
Available online 11 November 2025
0008-6215/© 2025 The Authors. Published by Elsevier Ltd. This is an open access article under the CC BY-NC-ND license (http://creativecommons.org/licenses/by-nc-nd/4.0/).

(2-keto-3-deoxy-α-D-*manno*-octulosonic acid) and heptose monosaccharides, and ii) an outer core, whose composition is more variable and includes hexoses, hexosamines, etc. Here, the LOS from *A. modestus* CM11G was isolated and its structure was characterised, revealing that lipid A is mainly composed of a heptacylated species. The OS region, on the other hand, is composed of a single internal Kdo residue substituted at position 4 with an external Kdo and at position five with a newly tetrasaccharide structure.

2. Materials and methods

2.1. Isolation and purification of LOS

A. modestus CM11G was isolated from the caecum and proximal colon tissues of a healthy mouse as described by Naito et al. [6,7]. The bacterium was grown by following the procedure reported on BacDive website, obtaining dry cells (8 g). Therefore, the LOS material was isolated from dry cells using the 90 % phenol-chloroform-petroleum ether (2:5:8 v/v/v; PCP) extraction [10,11], following the *Scheme* in Fig. 1. The slurry was then centrifuged (at 4 °C, 2060 *g* for 10 min), obtaining a supernatant and a pellet, which was saved for further extractions. After removing the low-boiling solvents from the supernatant, the LOS material was precipitated from the phenol solution by adding a few drops of water. A white flocculent was recovered by centrifugation (4 °C, 4630 *g*, 10 min), resuspended in water and dialyzed (cut-off 12–14 kDa) against Milli-Q water (Precipitate A). Analogously, the phenol phase was dialyzed, observing the formation of a precipitate (B), which was removed (*Scheme* in Fig. 1). All fractions (LOS material (A), precipitate (B) and supernatant (C) of phenol phase after dialysis) were freeze-dried, obtaining a yield of 0.8 %, 4.5 % and 0.3 % g/g_{cells}, respectively. The PCP pellet was subjected to hot phenol/water extraction [12]. Briefly, the wet pellet is dissolved in 90 % aqueous phenol/water (1:1 v/v) and stirred at 70 °C for 30 min, after which a centrifugation, at 4 °C, was performed, obtaining three phases (phenol phase, a milky interphase and water phase). The water phase was replaced with a fresh one and the extraction was repeated twice. The water phase obtained (D) was dialyzed as described above and then freeze-dried, obtaining 1.215 g (15.2 % yield). The phenol phase was dialyzed as described above and then centrifuged (4 °C, 260 g for 10 min), obtaining a pellet (3,75 g) and a phenol phase (E) 0.45 g (5.6 % yield). All fractions obtained were screened via SDS-PAGE [13] by using a polyacrylamide gel at 12 %. A silver nitrate staining was performed detecting the presence of LOS molecules in the precipitate of PCP and in both aqueous and phenol phases of water/phenol extraction (lanes **A**, **D** and **E** of Fig. 1). A pure LOS was obtained exclusively from the PCP precipitate (A). In contrast, contaminations were evident in the water and phenol phases of the water/phenol extractions due to the presence of additional bands at higher molecular weights. Therefore, the LOS obtained from the PCP precipitate (A) was used for further analysis.

2.2. Compositional analysis

Sugar compositional analysis was elucidated by derivatizing the LOS sample as peracetylated O-methyl glycosides (AMG) as described elsewhere [11,26]. Briefly, methanolysis (1.25 M HCl/MeOH, 80 °C, 16 h) followed by extraction with n-hexane and acetylation of the methanol phase (acetic anhydride in pyridine, 80 °C for 30 min) was performed. The organic phase obtained from the hexane extraction contains lipids derivatized as fatty acid methyl esters (FAME), which can be directly analyzed by GC-MS. The absolute configuration of each monosaccharide was inferred by analyzing their acetylated 2-(−)-octyl derivatives (AOG) [14,15]. Briefly, the sample was first dissolved in 100 μL of enantiopure 2-octanol and 14 μL of acetyl chloride and incubated at 60 °C for 16 h, and then the acetylation was performed. Since the OS region might contain hexosamines and their derivatization as octyl diastereoisomers coelutes, the 2-butanol derivatization was also performed to avoid the loss of important information. The monosaccharide substitution pattern was established derivatizing the OS region, obtained with the procedure described in paragraph 2.4, into partially methylated alditol acetate (PMAA), that consists of four steps: methylation (iodomethane and a spatula of NaOH for 16 h), acid hydrolysis (2 M TFA at 120 °C for 2 h), reduction (spatula of $NaBD_4$, at 25 °C for 16 h) and acetylation (as described before) [11].

All experiments were carried out on an Agilent Technologies Gas Chromatograph 6850A interfaced with Mass Spectrometry: a selective Mass Detector 5973 N. The gas chromatograph is equipped with an SPB-5 capillary column (Supelco, 30 m × 0.25 i.d., flow rate, 0.8 mL min^{-1}) using He as the carrier gas (flow rate: 1 mL min^{-1}; acquisition delay: 3 min). Electron impact mass spectra were recorded with an ionization energy of 70 eV and an ionizing current of 0.2 mA. All analyses were performed by using the following temperature program (150 °C for 5 min, 150 up to 280 °C at 3 °C/min, and 300 °C for 5 min) except for C8:0 (3-OH), a very short fatty acid, for which the following one was set (80 °C for 4 min, 10 °C/min up to 280 °C). Acetone is used as the solvent to dissolve all samples.

2.3. Oligosaccharide portion isolation

Total delipidation procedure of the LOS was performed as reported in Gargiulo et al. [16]. Briefly, 38 mg of the pure LOS material (Precipitate A, Fig. 1) was deesterified by hydrazinolysis (1 M hydrazine for 1h at 37 °C). Thus, the solution was poured into cold acetone and the de-*O*-acetylated LOS was collected by centrifugation, washed, and precipitated with cold acetone. Therefore, the precipitate (around 11 mg) was deacylated with a strong alkaline hydrolysis (1 ml of 4 M KOH, for 16 h at 120 °C) and then desalted by size-exclusion chromatography (SEC) on a Sephadex G10 (volume: 129 cm^3, flow: 12.5 mL/h, using Milli-Q water as eluent). The eluate was monitored by a refractive index detector (Knauer K-2310), and fractions were pooled accordingly and checked via proton NMR. A pure delipidated LOS was obtained in the initial part of the column, yielding 4 mg.

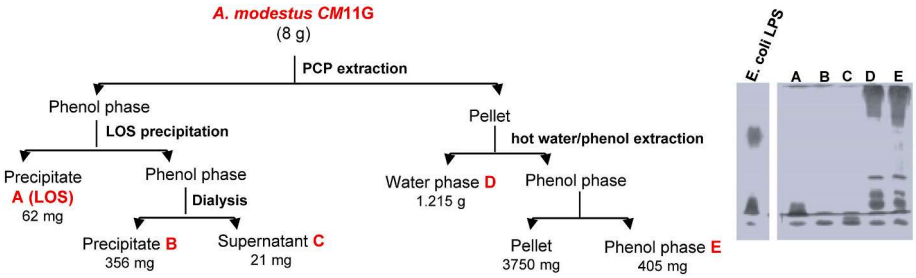

Fig. 1. Purification scheme of LOS from *A. modestus* CM11G. All obtained fractions were analyzed via SDS-PAGE (in the insert) using a polyacrylamide gel at 12 % and silver staining. LPS of. *E. coli* O111 was used as a reference, while lines **A** to **E** are named according to the respective fractions as indicated in scheme. 12 μg of each sample was loaded on the gel. Details about the two extractions and the centrifugations are reported in the 1.1 paragraph.

2.4. Isolation of lipid A and ammonia-deacetylated derivatization

The lipid A was isolated from pure LOS (5 mg) by mild acid hydrolysis (10 mg LOS/1 ml of acetic acid 1 % incubated at 100 °C). Once the precipitation of a white flocculent was observed (after 1 h), the reaction was stopped and the precipitate (lipid A) recovered by centrifugation (4630 *g*, 15 min at 25 °C), freeze-dried (1,39 mg) and used for structural investigation via MALDI-TOF mass spectrometry. The supernatant contains only the oligosaccharide portion of the OS region (2 mg), which was used for compositional analysis. To completely elucidate the lipid A structure of *A. modestus,* an aliquot was treated with ammonia as reported in Silipo et al. [17], followed by a selective removal of the ester bond fatty acid with sodium hydroxide treatment (NaOH 0,5 M for 2h at 37 °C) [18].

2.5. NMR acquisition parameters

^{1}H and ^{13}C NMR spectra were recorded in D_2O, at 308 K, on a Bruker 600 DRX spectrometer equipped with a cryo-probe, using acetone as internal standard (d_H 2.225 ppm and d_C 31.45 ppm). Homonuclear experiments were recorded using 512 FIDs of 2048 complex with 32 scans per FID for TOCSY and COSY. A mixing time of 100 ms was used for TOCSY spectrum acquisition. HSQC, HMBC and HSQC-TOCSY spectra were acquired with 512 FIDs of 2048 complex point, accumulating 40, 80 and 80 scans, respectively. All spectra were processed and analyzed using a Bruker TopSpin 3 program.

2.6. MALDI TOF mass spectrometry analysis

MALDI-TOF mass spectra of lipid A were acquired in negative and positive polarity using a 4800 Proteomic Analyzer (Applied Biosystems) equipped with a Nd:YAG laser (λ = 355 nm), with a mass accuracy of ~50 ppm [9]. 2,4,6-trihydroxyacetophenone (THAP) dissolved at a concentration of 75 mg/mL in methanol/0.1 % TFA/acetonitrile (ratio 7:2:1 v/v/v) was used as the matrix in MS Reflector mode, while MS/MS spectra were acquired using 5-chloro-2-mercaptobenzothiazole dissolved in methanol/water (4:1 v/v) 10 mg/ml 8. 1 μL of the matrix/-sample mixture (1:1 v/v) was deposited onto a MALDI plate and allowed to dry. In the MS experiments, each spectrum resulted from the accumulation of 2000 laser shots, whereas 5000–10,000 shots were summed for the MS/MS data acquisitions. Analyses were performed in triplicate and data processed with DataExplorer™ v4.9.

3. Result and discussion

3.1. LOS extraction

The lipooligosaccharide (LOS) from *A. modestus* CM11G was extracted from dried cells through a sequential phenol/chloroform/petroleum ether (PCP) [10] and hot phenol/water [11] extractions (*Scheme* in Fig. 1), as detailed in the materials and methods section. Both extractions allowed the isolation of the LOS material, although with different degrees of purity, as evident from the SDS-PAGE analysis (Fig. 1). Indeed, the PCP precipitate (lane **A** of gel in Fig. 1) shows pure LOS material, while the water and phenolic phases of the phenol/water extraction (lanes **D** and **E**) exhibited bands at high molecular weight, suggesting the presence of contamination from nucleic acids, proteins and/or high molecular weight polysaccharides. For this reason, the LOS obtained from PCP extraction was used for further analysis.

3.2. Compositional analysis

The preliminary monosaccharide composition of LOS was established from acetylated *O*-methyl glycosides (Fig. S1A). Glucose (Glc), galactose (Gal), glucosamine (GlcN) and 3-deoxy-D-*manno*-2-octulosonic acid (Kdo) were the main sugar components (Fig. S1A). As for the absolute configuration, both octyl- and butyl-glycoside derivatives established that all monosaccharides had the D configuration, except for Kdo, for which it was not determined. Regarding the fatty acids content, instead, the analysis revealed the presence of short fatty acid chains: C10:0, C12:0, C12:0 2OH, C12:0 3OH and C14:0 (data not shown). Information on the substitution pattern of monosaccharides in the OS region was retrieved by derivatizing this portion into partially methylated alditol acetate (Fig. S1B). Galactose was substituted at position 2, glucosamine was present as terminal sugar (t-GlcN), while glucose was present as both terminal monosaccharide (t-Glc) and 4,6-linked (4,6-Glc) (Fig. S1B).

3.3. Structural characterization of the delipidated LOS

An aliquot of pure LOS was completely delipidated, following the procedure reported in paragraph 2.3, to establish the structure of the glycan portion. Therefore, pure LOS was first deesterified by hydrazinolysis and then deacylated by strong alkaline hydrolysis, thus obtaining an oligosaccharide fraction which was purified by size exclusion chromatography using a Sephadex G-10. Proton NMR of all column fractions revealed the presence of the pure oligosaccharide in the initial part of the column, as expected.

The ^{1}H NMR profile of the oligosaccharide fraction (Fig. 2) shows six distinct anomeric signals ranging from 5.6 to 4.5 ppm, labelled **A** to **F**, and a crowded carbinolic region (4.3–3.3 ppm). Furthermore, typical signals of protons H-3 from two Kdo residues (between 1.8 and 2.0 ppm) were found (**Ka$_{3ax}$** and **Kb$_{3ax}$** in Fig. 2).

The spin system of all residues was assigned (Table 1) by studying a full set of bidimensional NMR spectra (COSY, TOCSY, HSQC, HSQC-TOCSY, HMBC). Residues **A** and **D** were recognized as glucosamine monosaccharides of the lipid A backbone ($GlcN_I$ and $GlcN_{II}$, respectively). The efficient magnetization transfer in the TOCSY spectrum from H-1 up to H-6 confirmed the *gluco* stereochemistry of these residues (Fig. S2). The configuration at the anomeric carbon was identified as α for residue **A** and β for residue **D**, based on literature data [19]. Indeed, the C5 and C3 carbon densities of residue **A** have chemical shift values of 73.4 ppm and 70.9 ppm, respectively, typical of a GlcN unit in the free reducing form [19]. The C3 and C5 carbon densities of residue **D**, instead, are compatible with those of a β-GlcN in not reducing form. In agreement, the anomeric proton of the residue **A** exhibits a duplet of doublets (dd) multiplicity ($^{3}J_{H1,H2}$ 3.3 Hz; $^{3}J_{H1,P}$ 9.5 Hz) that is typical of the $GlcN_I$ being phosphorylated at position O-1, as further indicated by the chemical shift value of the anomeric carbon at 92 ppm [19]. J coupling constant $^{3}J_{H1,H2}$ of the residue **A** is small, 3.3 Hz, typical of an alpha anomeric carbon. On the contrary, the anomeric proton of the residue **D** appears as a doublet, with a large J coupling constant of 8.5 Hz, typical of a β anomeric carbon. Furthermore, the HSQC spectrum (Fig. 3) showed that the carbon C6 of both residues resonated at lower fields compared to those of the unsubstituted residue (71.1 ppm and 63.8 ppm, respectively) [20], indicating that these positions are glycosylated. As usual, $GlcN_{II}$ (residue **D**) is linked at O-6 of the $GlcN_I$ (residue **A**), as demonstrated by the HMBC correlations between H-1 of **D** with C-6 of **A.** (Fig. 3). Instead, the chemical shift value of C-6 of residue **D** is compatible with a substitution with a ketose unit [19], as evident from the mild glycosylation effect (63.8 ppm against 62 ppm in the unsubstituted residue [19].

Residues **B** and **F** were instead assigned to a 4,6-linked and a terminal glucose, respectively. The *gluco* stereochemistry of these residues was deduced by the efficient magnetization transfer in the TOCSY spectrum (Fig. S2), similarly to residues **A** and **D**. Assigning the chemical shift values of protons H-3, H-4 and H-5 of residue **F** was challenging, since they are overlapped. However, the corresponding carbons were identified using HSQC-TOCSY (Fig. S3), giving the possibility to distinguish between them. The **B** residue is α configurated at the anomeric carbon as inferred from the small coupling constant $^{3}J_{H1,H2}$ (3.05 Hz), while **F** was β configured as denoted from a large coupling constant $^{3}J_{H1,H2}$ (7.6 Hz).

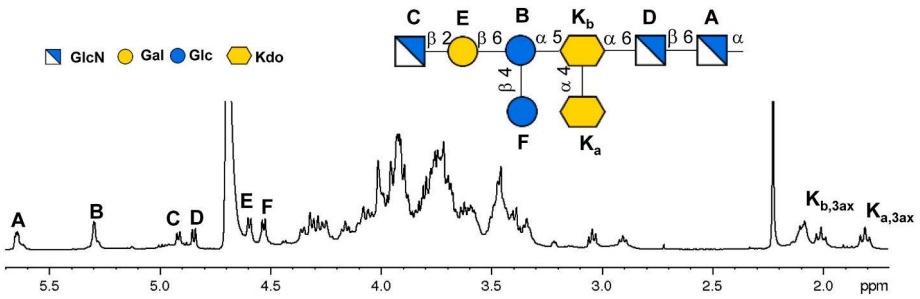

Fig. 2. (600 MHz, 308 K, D_2O). ^1H NMR analysis of totally deacylated LOS of *A. modestus* CM11G. The letters follow the system of Table 1. The structure is represented according to the symbol as defined by the rules of the Symbol Nomenclature For Glycans (SNFG).

Table 1
Proton and carbon chemical shift values of the OS region of the LOS of *A. modestus* CM11G.

		1	2	3	4	5	6	7	8
A	^1H	5.65	3.39	3.90	3.62	4.12	4.30/3.75	–	–
6−α-GlcN$_I$	^{13}C	91.9	55.9	70.9	70.9	73.4	71.1	–	–
B	^1H	5.29	3.59	3.96	3.95	4.35	4.26/4.08	–	–
4,6-α-Glc	^{13}C	100.1	73.0	72.3	80.7	70.5	68.6	–	–
C	^1H	4.91	2.90	3.61	3.38	3.48	3.94/3.77	–	–
t-β-GlcN	^{13}C	102.6	58.3	74.8	71.3	77.8	61.9	–	–
D	^1H	4.85	3.04	3.84	3.73	3.72	3.70/3.46	–	–
6−β-GlcN$_{II}$	^{13}C	100.9	56.9	73.7	74.6	75.5	63.8	–	–
E	^1H	4.59	3.79	3.88	3.91	3.68	~3.73	–	–
2-β-Gal	^{13}C	102.6	80.2	74.5	70.2	76.3	64.1	–	–
F	^1H	4.53	3.34	3.46	3.46	3.44	3.95/3.75	–	–
t-β-Glc	^{13}C	104.1	74.3	76.8	70.7	77.3	61.9	–	–
Ka	^1H	–	–	2.08/1.81	3.99	4.01	3.71	4.00	3.94/3.75
α-Kdo	^{13}C	176.0	103	35.9	67.3	68.0	73.2	71.7	64.0
Kb	^1H	–	–	2.10/2.00	4.10	4.32	3.75	4.04	3.90/3.67
4,5-α-Kdo	^{13}C	176	101	35.9	72.1	74.8	73.6	70.1	64.6

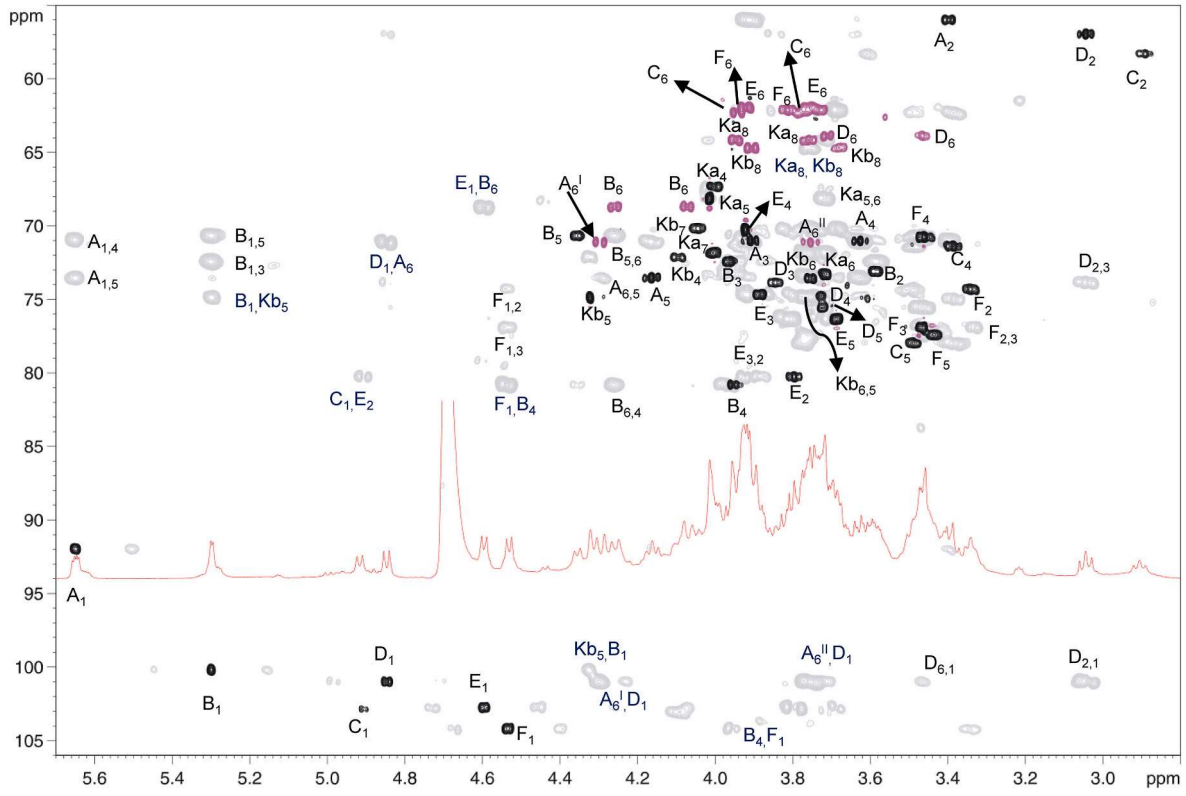

Fig. 3. (600 MHz, 308 K, D_2O). Overlay of HMBC (grey) and HSQC (black and pink) spectra of delipidated LOS from *Acinetobacter modestus* CM11G. Significant HMBC correlations are shown in blue. The letters follow the scheme of Table 1. (For interpretation of the references to colour in this figure legend, the reader is referred to the Web version of this article.)

The low-field shift of both carbons C-4 (80,7 p.m.) and C-6 (68,6 ppm) compared to those of the unsubstituted residue (70.6 ppm and 61.8 ppm, respectively [20]) suggested that the residue **B** was substituted at positions 4 and 6. Information confirmed by the clear correlations between the H-1 of **E** with the C-6 of **B** and the H-1 of **F** with the C-4 of **B**, in the HMBC spectrum (Fig. 3).

As for the **C** residue, it has been identified as a terminal β glucosamine. Analogously to the previous monosaccharides, the efficient magnetization transfer in the TOCSY spectrum indicated that this residue also possesses a *gluco* stereochemistry. The anomeric signal at 4,91 ppm appears as a doublet with a large coupling constant $^{3}J_{H1,H2}$ (8.5 Hz), a typical signature of a sugar β-configured at the anomeric carbon. Combining all the NMR data, it was possible to assign all the chemical shift values of the protons and carbons, resulting in values similar to those of an unsubstituted residue [20] and, therefore, identifying it as a terminal unit.

Regarding the residue **E**, it's *galacto* stereochemistry was inferred from the TOCSY spectrum which showed a correlation from H-1 up to H-3 (Fig. S2). Moreover, the large J coupling constant $^{3}J_{H1,H2}$ (8.6 Hz) indicates a β configuration at the anomeric carbon. Furthermore, the carbon density C2 resonates at a lower field (80.2 ppm) than that of unsubstituted galactose (71.7 ppm) [20], suggesting that residue **E** was glycosylated at position 2. This is also confirmed by the HMBC correlation between the H-1 of **C** with the C-2 of **E** (Fig. 3).

Two Kdo residues were identified, labelled **Ka** and **Kb.** The HMBC spectrum displayed correlations between H-3 and up to C-5, between H-5 and C-6, and between H-7 and C-8 for both residues (Fig. 3 and S4). The HSQC spectrum showed that the carbons C-4 and C-5 of the residue **Kb** are compatible with the chemical shift values of the Kdo substituted at those positions [19]. This data agrees with the HMBC correlations between the H-1 of B and C-5 of **Kb** (Fig. 3). Additionally, the C-4 chemical shift value of **Kb** is compatible with a substitution with a ketose unit, namely **Ka** [19]. In agreement, the HMBC correlation between the H-8 of Ka and C-8 of Kb, and H-3eq. of **Kb** with C-4 and C-5 of **Ka** (Fig. S4), suggests that the two Kdo residues are spatially close, thus placing **Ka** on the O-4 of **Kb**. Conversely, Ka was attributed as a terminal Kdo residue based on the carbon chemical shift values (Table 1) [19.]. The α configuration of both residues was established based on the chemical shift values for the H-3eq protons (2.10 ppm and 2.08 ppm, respectively, for **Kb** and **Ka**) [19]. Consequently, **Ka** represent the external Kdo unit, while **Kb** is the internal one linked to the O-6 of the $GlcN_{II}$ residue (**D**) in agreement with the chemical shift value of C-6 of residue **D**.

Combining all the spectroscopic data, the structure of the OS of

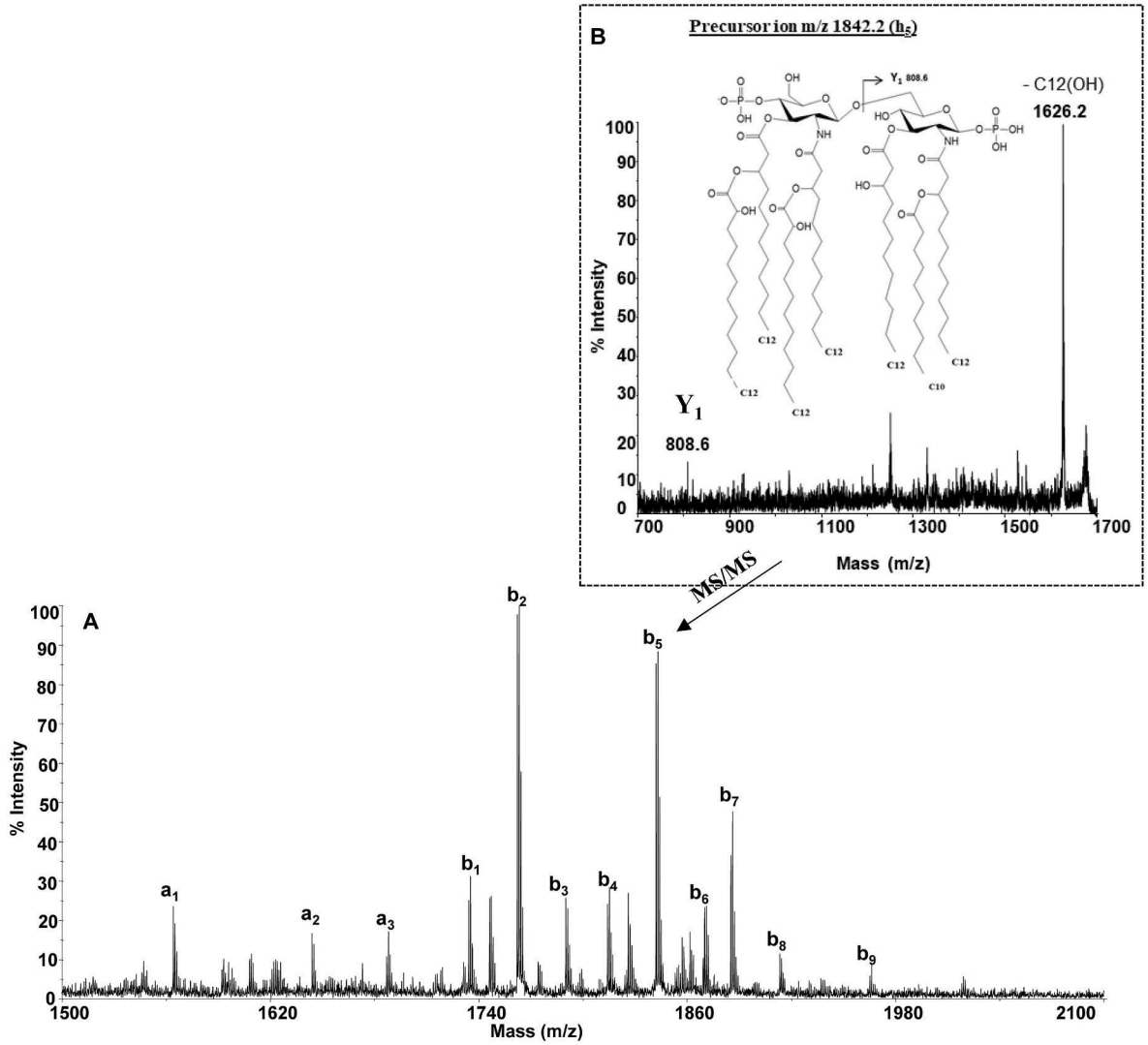

Fig. 4. A) Negative-ion reflector MALDI mass spectrum of *Acinetobacter modestus* lipid A. The ion groups **a** and **b** correspond to the hexa and hepta-acylated species, respectively. The composition of each peak is reported in Table S1. **B)** MALDI MS/MS spectrum of the bis-phosphorylated hepta-acylated lipid A species ($\mathbf{b_5}$ *m/z* 1842.2). The structure of lipid A is shown in the figure.

A. modestus CM11G was fully elucidated (schematized in Fig. 2). The disaccharide of D-glucosamine linked via β(1→6) glycosidic bond is connected to the oligosaccharide moiety via an internal Kdo residue (**Kb**) which is elongated at the *O*-4 position with an external Kdo (**Ka**) and at the *O*-5 position by a linear trisaccharide of βGlcN(1→2)-βGal (1→6)-αGlc(1→), where glucose is further substituted at the position 4 with a terminal β-glucose.

3.4. Lipid A structural determination

The lipid A of *A. modestus* was isolated by treating the pure LOS with mild acid hydrolysis, as detailed in paragraph 2.3 and used for studies.

MALDI-MS analysis in negative mode (Fig. 4A) clearly showed two sets of deprotonated molecular ions $[M-H]^-$, which were assigned to the hexa-acyl (group **a**) and hepta-acyl (group **b**) species, where the latter is predominant. Hexa-acyl species $\mathbf{a_1}$ (*m/z* 1564.0) was attributed to a mono-phosphorylated, lipid A carrying five C12:0(OH) and one C10:0. Species $\mathbf{a_2}$ (*m/z* 1644.0) was identified as the analogous bis-phosphorylated species (Δ*m/z* 80). The peak at *m/z* 1687.0 ($\mathbf{a_3}$) differs from $\mathbf{a_2}$ by Δ*m/z* 43, corresponding to the replacement of one phosphate group with a 2-aminoethyl phosphate (PEtN) group.

The base peak at *m/z* 1762.2 ($\mathbf{b_2}$) was assigned to a mono-phosphorylated, hepta-acylated lipid A species carrying six C12:0(OH) and one C10:0, while the peak at *m/z* 1842.2 ($\mathbf{b_5}$) was identified as the bis-phosphorylated analogue (Δ*m/z* 80).

Peaks at *m/z* 1885.2 ($\mathbf{b_7}$) and at *m/z* 1965.2 ($\mathbf{b_9}$) differ from $\mathbf{b_2}$ and $\mathbf{b_5}$ by an additional PEtN group (Δ*m/z* 123). Starting from $\mathbf{b_2}$ and $\mathbf{b_7}$, the composition of all the hepta-acylated lipid A species could be deduced (Table S1).

The composition of the hexa- and hepta-acylated lipid A species revealed that each of the two GlcN residues contains a C12:0(3-OH) primary fatty acid, which is attached via an ester and an amide bond. This composition was validated by analysing the MS/MS spectrum (Fig. 4B) of the parent ion at *m/z* 1842.2 ($\mathbf{b_5}$), representing the main bis-phosphorylated hepta-acylated lipid A species. Notably, an abundant ion at *m/z* 1626.6 was observed, indicating the loss of C12:0(3-OH) consistent with the compositional analysis. The peak at *m/z* 808.6 (Fragment **Y1**), generated by cleavage of the glycosidic linkage between the two GlcN residues, was also significant. An aliquot of lipid A was treated with NH_3 aq to effectively remove the ester-linked acyloxyacyl esters, thereby definitively establishing the location of C10:0 [15]. The MALDI spectrum of the ammonia-treated lipid A (Fig. S5) displayed an abundant ion at *m/z* 1247.7, matching the glucosamine backbone with two phosphate groups, three C12:0(OH) groups and one C10:0 group. The peak at *m/z* 1167.7 was attributed to the corresponding mono-phosphorylated species. The presence of C10:0 following ammonia treatment indicates that this fatty acid is linked to the amide-bound C12:0(3-OH) of $GlcN_I$.

In addition, a peak at *m/z* 1195.8 was detectable. This is composed of two GlcN, one phosphate group, three C 12:0(OH) and one C 12:0. The peak at *m/z* 1275.7 was identified as the corresponding bis-phosphorylated species. Therefore, we can conclude that the C10:0 and C12:0 are linked to the amide-linked C12:0(3-OH).

These data were confirmed by analysing the positive-ion MALDI spectrum of O-deacylated lipid A under mild conditions (Fig. S6). This spectrum showed several ion peaks corresponding to partially and completely O-deacylated lipid A species. Specifically, the peaks at *m/z* 839.4 and 861.4 represent the glucosamine backbone mono-phosphorylated with amide-linked primary fatty acids, C12:0(3-OH), lacking secondary fatty acids, $[M+Na]^+$ and $[M+2Na-H]^+$ adducts, respectively (Fig. S6A). In contrast, the peaks at *m/z* 1043.5 ($[M+2Na-H]^+$ adduct) and 993.5 ($[M+Na]^+$) corresponded to partially deacylated lipid A species that still bore one C12:0 and one C10:0 fatty acid as secondary fatty acids, respectively. The peak at *m/z* 993.5 was investigated by MS/MS (Fig. S6B). The resulting spectrum showed, besides the B-ion [21] at 462.2, two peaks at *m/z* 554.3 and *m/z* 582.2 originating from the sugar ring fragmentations $^{0.3}A_2$ and $^{0.2}A_2$, respectively These fragmentations confirmed the exact location of C10:0 on $GlcN_I$.

Combining MALDI mass spectrometry information with compositional analysis, we can conclude that the hexa- and hepta-acylated lipid A species of *A. modestus* consisted of $GlcN_{II}$, which had two C12:0(3-OH) as primary fatty acids and two or one C12:0(2-OH) as secondary fatty acids. $GlcN_I$ had the same pattern of primary fatty acids, but only one secondary fatty acid, which could be C10:0 or C12:0 (Fig. S7).

4. Conclusion

In recent years, a lot of effort has been made to characterize the structure of the capsular polysaccharides produced by different strains of *A. baumannii*, a strong virulence factor, revealing the occurrence of peculiar non-ulosonic acid never found before [22]. In contrast, the LOS has been characterized only for a few *A. baumannii* strains [23,24]. As example, *A. baumannii ATCC* 19606 produces a LOS composed of a lipid A moiety which is connected via a Kdo trisaccharide (two internal Kdo and one external Kdo residue) to the oligosaccharide portion (outer core), which consists of six monosaccharides [24]. Generally, the inner core is preserved across different strains of the same species, while the outer core is the most variable part. To the best of our knowledge, the structure of the LOS of non-pathogenic *Acinetobacter* species has never been reported.

In the present study, we reported for the first time the chemical structure of the LOS of *A. modestus* CM11G, a non-pathogenic *Acinetobacter*, colonizing the intestinal crypts of a healthy mouse. The lipid A is connected to the OS region by a disaccharide of Kdo, as occurs for *A. baumanni* ATTC 17905, where only the internal Kdo is further elongated with a tetrasaccharide. Contrary to the other *A. baumannii* strains, in which the external Kdo residue is further substituted with a monosaccharide [23] or a linear trisaccharide [23], here it is unsubstituted. Interestingly, a novel structure is exhibited by the tetrasaccharide that constitutes the outer core of *A. modestus*. Indeed, comparing this structure with those deposited in the CSDB database (search conducted on July 30, 2025) results that it is new, albeit it is constituted by "normal" sugars (Fig. 2): glucose, galactose and glucosamine. Monosaccharides that are also found in the outer core of *A. baumanni* strains [23,24].

Regarding the lipid A portion of *A. modestus*, instead, it is mainly constituted by hexa and hepta-acylated species, where the hepta-acylated is the predominant one, in accordance with other *Acinetobacter* species [25]. Both species possess a $GlcN_{II}$ acylated with C12 (3OH) as primary fatty acids and with one or two C12:0(2OH) as secondary fatty acids. The $GlcN_{II}$ and the $GlcN_I$ differ only in the acylation pattern of the secondary fatty acid, which is only one, namely C10:0 or C12:0, according to the species considered (Fig. S7).

As stated in the literature, the structure of the lipid A of another non-pathogenic *Acinetobacter*, *A. radioresistans* S13, is composed of tetra-, penta-, hexa- and hepta-acylated species. While the hepta-acylated species is the dominant one, the hexa-acylated species is also present in a reasonable amount, in contrast to that of *A. modestus*. Furthermore, a closer look at the fatty acid compositions reveals some minor differences, such as the absence of a C14:0(3OH) as a primary fatty acid and the occurrence of a C10:0 as a secondary fatty acid in the lipid A of *A. modestus* CM11G.

This study lays the foundation for future investigations on the biological role of lipooligosaccharides, including both the lipid A and oligosaccharide regions, produced by the Gram-negative bacteria inhabiting the crypt-specific core microbiota of healthy mice. Ultimately, this investigation represents a first step in understanding whether and how distinctive structural features influence their functional behaviour.

CRediT authorship contribution statement

Immacolata Speciale: Writing – review & editing, Writing – original draft, Methodology, Investigation, Formal analysis. **Luisa Sturiale:** Methodology, Investigation, Formal analysis. **Angelo Palmigiano:** Visualization, Methodology, Investigation, Formal analysis. **Anna Notaro:** Writing – review & editing, Writing – original draft, Visualization, Supervision, Investigation.

Declaration of competing interest

The authors declare that they have no known competing financial interests or personal relationships that could have appeared to influence the work reported in this paper.

Acknowledgment

The authors would like to express their sincere gratitude to Thierry Pedron of the Institut Pasteur in Paris, France, for kindly providing them with the *A. modestus* CM11G, which was isolated from the caecum and proximal colon tissues of healthy mice.

This research did not receive any specific grant from funding agencies in the public, commercial, or not-for-profit sectors.

Appendix A. Supplementary data

Supplementary data to this article can be found online at https://doi.org/10.1016/j.carres.2025.109743.

Data availability

Data will be made available on request.

References

[1] T. Muleshkova, I. Bazukyan, K. Papadimitriou, V. Gotcheva, A. Angelov, S. G. Dimov, J. Microbiol. Biotechnol. 35 (2025) e2411043.
[2] J. Jung, E.L. Madsen, C.O. Jeon, W. Park, Appl. Environ. Microbiol. 77 (2011) 7418–7424.
[3] Y. Zhan, Y. Yan, W. Zhang, M. Chen, W. Lu, S. Ping, M. Lin, Res. Microbiol. 163 (2012) 36–43.
[4] C. Ayoub Moubareck, D. Hammoudi Halat, Antibiotics (Basel, Switzerland) 9 (2020) 119.
[5] T. Pédron, C. Mulet, C. Dauga, L. Frangeul, C. Chervaux, G. Grompone, P. J. Sansonetti, mBio 3 (2012) e00116, 12.
[6] A. Saffarian, M. Touchon, C. Mulet, R. Tournebize, V. Passet, S. Brisse, E.P. C. Rocha, P.J. Sansonetti, T. Pédron, BMC Genom. 18 (2017) 525.
[7] T. Naito, C. Mulet, C. De Castro, A. Molinaro, A. Saffarian, G. Nigro, M. Bérard, M. Clerc, A.B. Pedersen, P.J. Sansonetti, T. Pédron, mBio 8 (2017).
[8] F. Di Lorenzo, K.A. Duda, R. Lanzetta, A. Silipo, C. De Castro, A. Molinaro, Chem. Rev. 122 (2022) 15767–15821.
[9] A. Notaro, L. Sturiale, A. Palmigiano, D. Garozzo, I. Speciale, Carbohydr. Res. 555 (2025) 109586.
[10] C. Galanos, O. Luderitz, O. Westphal, Eur. J. Biochem. 9 (1969) 245–249.
[11] C. De Castro, M. Parrilli, O. Holst, A. Molinaro, Methods Enzymol. 480 (2010) 89–115.
[12] O. Westphal, K. Jann, Methods in carbohydrate, Chemistry 5 (1965) 83–91.
[13] U.K. Laemmli, Nature 227 (1970) 680–685.
[14] K. Leontein, B. Lindberg, L. Lonngren, Carbohydr. Res. 62 (1978) 359–362.
[15] P. Garcia-Vello, I. Speciale, F. Di Lorenzo, A. Molinaro, C. De Castro, Methods Mol. Biol. 2548 (2022) 181–209.
[16] V. Gargiulo, D. Garozzo, R. Lanzetta, A. Molinaro, L. Sturiale, C. De Castro, M. Parrilli, Chembiochem 9 (2008) 1830–1835.
[17] A. Silipo, R. Lanzetta, A. Amoresano, M. Parrilli, A. Molinaro, J. Lipid Res. 43 (2002) 2188–2195.
[18] E. Fregolino, G. Fugazza, E. Galano, V. Gargiulo, P. Landini, R. Lanzetta, B. Lindner, L. Pagani, M. Parrilli, O. Holst, C. De Castro, Eur. J. Org Chem. (2010) 1345–1352.
[19] C. De Castro, A. Carannante, R. Lanzetta, B. Lindner, R. Nunziata, M. Parrilli, O. Holst, Chemistry 12 (2006) 4668–4674.
[20] I. Speciale, A. Notaro, P. Garcia-Vello, F. Di Lorenzo, S. Armiento, A. Molinaro, R. Marchetti, A. Silipo, C. De Castro, Carbohydr. Polym. 277 (2022) 118885.
[21] B. Domon, C.E. Costello, Glycoconj. J. 5 (1988) 397–409.
[22] J.J. Kenyon, A. Notaro, L.Y. Hsu, C. de Castro, R.M.J.S.R. Hall, 7 (2017).
[23] E.V. Vinogradov, K. Bock, B.O. Petersen, O. Holst, H. Brade, Eur. J. Biochem. 243 (1997) 122–127.
[24] D.R. Klein, M.J. Powers, M.S. Trent, J.S. Brodbelt, Anal. Chem. 91 (2019) 9608–9615.
[25] S. Leone, L. Sturiale, E. Pessione, R. Mazzoli, C. Giunta, R. Lanzetta, D. Garozzo, A. Molinaro, M. Parrilli, J. Lipid Res. 48 (2007) 1045–1051.
[26] A. Notaro, O. Poirot, E.D. Garcin, S. Nin, A. Molinaro, M. Tonetti, C. De Castro, C. Abergel, microLife 3 (2022).